Mineralogical Magazine (2019), **83**, 393–400
doi:10.1180/mgm.2018.129

CAMBRIDGE UNIVERSITY PRESS

Article

Pampaloite, AuSbTe, a new mineral from Pampalo gold mine, Finland

Anna Vymazalová[1]*, Kari Kojonen[2], František Laufek[1], Bo Johanson[3], Chris .J. Stanley[4], Jakub Plášil[5] and Patricie Halodová[1]

[1]Czech Geological Survey, Geologická 6, 152 00 Prague 5, Czech Republic; [2]Merivirta 6 B 36, FI- 02320 Espoo Finland; [3]Geological Survey of Finland, P.O.Box 96, FI-02151 Espoo, Finland; [4]Department of Earth Sciences, Natural History Museum, London SW7 5BD, UK; and [5]Institute of Physics, AS CR v.v.i. Na Slovance 2, 182 21, Prague 8, Czech Republic

Abstract

Pampaloite, AuSbTe, is a new mineral discovered in the Pampalo gold mine, 65 km east of Joensuu, Finland. It forms anhedral grains (up to ~20 μm) intergrown with gold, frohbergite and altaite. Pampaloite is brittle and has a metallic lustre. Values of VHN_{25} lie between 245 and 295 kg/mm^2, with a mean value of 276 kg/mm^2, corresponding to a Mohs hardness of ~4–5 (measured on synthetic material). In plane-polarised light, pampaloite is white with medium to strong bireflectance, weak reflectance pleochroism from slightly pinkish brown to slightly bluish white (only visible in grains of synthetic material containing multiple orientations), and strong anisotropy, with blue to light brown rotation tints; it exhibits no internal reflections. Reflectance values of pampaloite in air (R_1, R_2 in %) are: 60.0, 62.5 at 470 nm, 62.5, 64.8 at 546 nm, 63.2, 65.6 at 589 nm and 63.7, 66.0 at 650 nm. Ten electron-microprobe analyses of natural pampaloite give an average composition: Au 44.13, Sb 27.44 and Te 28.74, total 100.31 wt.%, corresponding to the empirical formula $Au_{1.00}Sb_{1.00}Te_{1.00}$ based on 3 atoms; the average of eleven analyses on synthetic pampaloite is: Au 44.03, Sb 27.26, and Te 29.08, total 100.38 wt.%, corresponding to $Au_{0.99}Sb_{1.00}Te_{1.01}$. The density, calculated on the basis of the empirical formula, is 9.33 g/cm^3.The mineral is monoclinic, space group $C2/c$, with $a = 11.947(3)$, $b = 4.481(1)$ Å, $c = 12.335(3)$ Å, $\beta = 105.83(2)°$, $V = 635.3(3)$ Å^3 and $Z = 8$. The crystal structure was solved and refined from the single-crystal X-ray-diffraction data of synthetic AuSbTe. The pampaloite crystal structure can be considered as a monoclinic derivative of the CdI_2 structure composed of $[AuTe_3Sb_3]$ octahedra. The strongest lines in the powder X-ray diffraction pattern of synthetic pampaloite [d in Å (I) (hkl)] are: 4.846(24)($\bar{2}02$), 3.825(18)(111), 2.978(100)($\bar{3}11$), 2.968(50)(004), 2.242(25)(020), 2.144(55)(313), 2.063(33)($\bar{3}15$) and 1.789(18)(024).

Keywords: pampaloite, AuSbTe, electron-microprobe, reflectance, X-ray-diffraction, crystal structure, Pampalo gold deposit, Finland

(Received 1 February 2018; accepted 19 April 2018; Accepted Manuscript online: 4 July 2018; Associate Editor: G. Diego Gatta)

Introduction

Pampaloite was discovered in drill core 315, at a depth of 71.50 m during exploration drilling at the Pampalo gold prospect (also called the Ward prospect), that was later developed as the Pampalo gold mine by Endomines AGM (Endomines, 2018). The Pampalo mine (Fig. 1) is located in eastern Finland close to the Russian border, 65 km east from Joensuu and 46 km north of Ilomantsi village (Nurmi *et al.*, 1993). The deposit is within the Archaean Hattu metasedimentary schist belt that extends 40 km south to north and continues on both directions across the Russian border to Eastern Karelia. The Hattu schist belt consists of hydrothermally altered and tectonically sheared biotite tonalities and metasedimentary epiclastic and felsic pyroclastic deposits (Fig. 1), hornblende-biotite granodiorites, submarine sulfide- and graphite-bearing metapelites altered to sericite schists, mafic and ultramafic rocks (soapstones and serpentinites), and quartz-feldspar porphyry dykes (Kojonen *et al.*, 1993). The Pampalo gold ore was located mainly in quartz–feldspar schist between metapelites and ultramafic intrusions (soapstones and serpentinites). Another gold ore type was found in the quartz–feldspar porphyry dykes. The gold ore lodes plunge 40° to the N. The deposit is still open in a N–S direction and more than 500 m deep (Endomines, 2018). The location of Pampalo drill core 315 is: 62°59'11"N, 31°15'53"E. A phase of similar composition is listed as an unnamed mineral (UM1984-41-Te:AuSb, Smith and Nickel, 2007).

Pampaloite is intergrown with altaite, frohbergite and native gold in an open space between the gangue minerals suggesting late hydrothermal crystallisation of Te- and Sb-bearing fluids (Johanson and Kojonen 1989; Kojonen *et al.*, 1993; 1994). The calaverite inclusions discovered in pyrite indicate high Te fugacity. Most of the gold grains found are intergrown with tellurides between the gangue minerals or in the fractures of pyrite. According to Afifi *et al.* (1988) this kind of Te-rich mineral paragenesis crystallised below 354°C, and typically below 250°C. Cabri (1965) gives even lower values of final equilibrium

*Author for correspondence: Anna Vymazalova, Email: anna.vymazalova@geology.cz
Cite this article: Vymazalová A., Kojonen K., Laufek F., Johanson B., Stanley C.J., Plášil J. and Halodová P. (2019) Pampaloite, AuSbTe, a new mineral from Pampalo gold mine, Finland. *Mineralogical Magazine* **83**, 393–400. https://doi.org/10.1180/mgm.2018.129

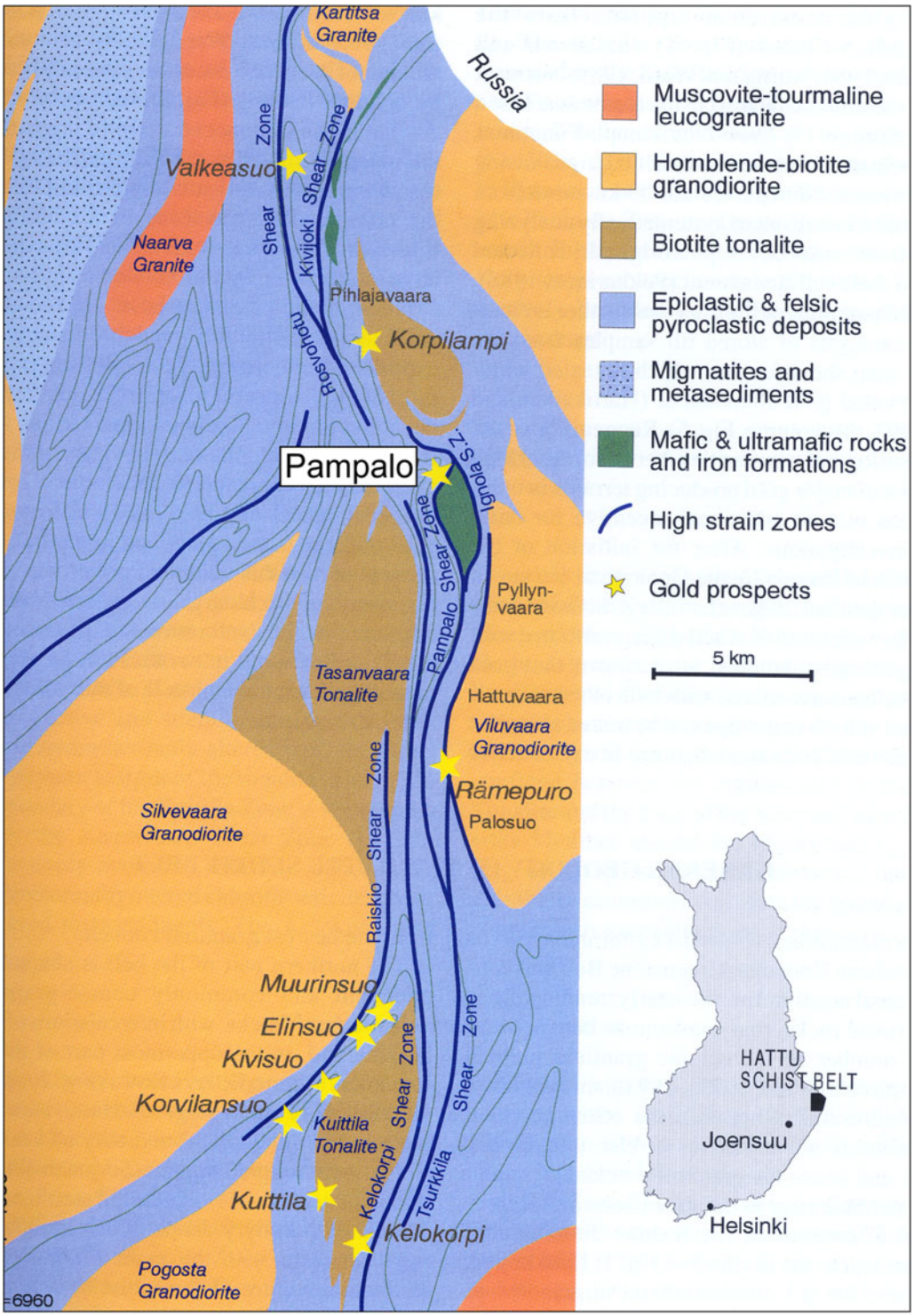

Fig 1. Geological map of the Hattu schist belt, Ilomantsi, Eastern Finland, adapted from Nurmi *et al.* (1993).

for a gold–hessite–petzite association at ~50°C. The formation of pampaloite at low temperatures is also in accordance within the experimental study of the Au–Sb–Te system by Nakamura and Ikeda (2002), where the AuSbTe phase was synthesised at 350°C.

Both mineral and name were approved by the Commission on New Minerals, Nomenclature and Classification of the International Mineralogical Association (IMA2017-096, Vymazalová *et al.*, 2018). The mineral is named for the locality, the Pampalo gold mine, Finland. The holotype (polished thin section) is deposited at the Department of Earth Sciences of the Natural History Museum, London, UK, catalogue No BM 2017, 16.

Appearance, physical and optical properties

Pampaloite forms anhedral grains (up to 20 μm in diameter) in aggregates with gold, frohbergite and altaite (Fig. 2). Other

https://doi.org/10.1180/mgm.2018.129 Published online by Cambridge University Press

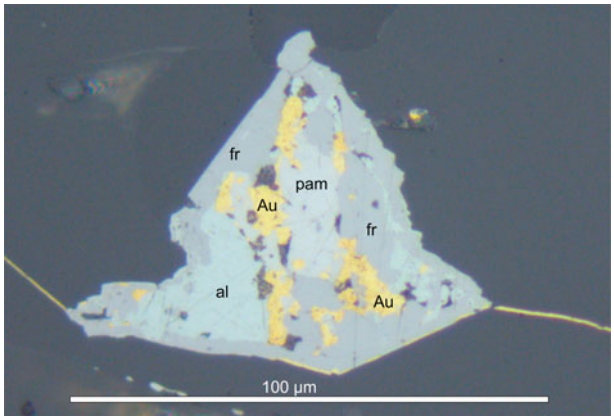

Fig. 2. Pampaloite (pam) intergrown with native gold (yellow) altaite (al) and frohbergite (fr). Microscope image, reflected polarised light. Sample No. Ku 18516.

ore minerals include pyrite, pyrrhotite, chalcopyrite, cubanite, galena, sphalerite, mackinawite, molybdenite, scheelite, rutile, tellurobismuthite, tsumoite, hessite, petzite, calaverite, volynskite, rucklidgeite, melonite, native bismuth, goethite, hematite, magnetite and chromite (Kojonen *et al.*, 1993). The most abundant gangue minerals are quartz, plagioclase, K-feldspar, biotite, muscovite, calcite and chlorite-group minerals; accessory minerals include garnet, staurolite, kyanite, tourmaline, rutile, titanite, apatite, zircon and epidote. The ultramafic wall rocks contain talc, carbonate, actinolitic amphibole, biotite and chlorite-group minerals.

Pampaloite is opaque with a metallic lustre. The mineral is brittle. Values of VHN_{25} measured from five indentations is in the range of 245 to 295 kg/mm^2 (measured on synthetic grains), with a mean value of 276 kg/mm^2, which corresponds to a Mohs hardness of ~4–5. The density calculated on the basis of the empirical formula is 9.33 g/cm^3. In plane-polarised reflected light, pampaloite is white (slightly bluish white in grains of synthetic material showing multiple orientations), has medium to strong bireflectance, weak reflectance pleochroism from slightly pinkish brown to slightly bluish white (only visible in grains of synthetic material containing multiple orientations), and strong anisotropy with blue to light brown rotation tints. It exhibits no internal reflections.

Reflectance measurements were made in air relative to a WTiC standard on both natural and synthetic pampaloite using a J & M TIDAS diode array spectrometer attached to a Zeiss Axiotron microscope. The results are tabulated (Table 1) and illustrated in Fig. 3.

Composition

Chemical analyses were performed with a CAMECA SX-100 electron probe microanalyser in wavelength-dispersive mode using an electron beam focussed to 1–2 µm. Pure elements were used as standards. Concentrations were quantified on Te*Lα*, Sb*Lα* and Au*Mα* with an accelerating voltage of 15 keV, and a beam current of 10 nA on the Faraday cup. Other elements were below the detection limit.

The electron-microprobe results are given in Table 2. The empirical formulae calculated on the basis of 3 apfu are $Au_{1.00}Sb_{1.00}Te_{1.00}$ for natural pampaloite and $Au_{0.99}Sb_{1.00}Te_{1.01}$ for its synthetic analogue, with ideal formulae AuSbTe.

Table 1. Reflectance data for natural and synthetic pampaloite.

	Natural		Synthetic	
λ (nm)	R_1 (%)	R_2 (%)	R_1 (%)	R_2 (%)
400	56.0	59.2	49.0	57.0
420	57.2	60.2	50.5	58.0
440	58.4	61.2	52.0	59.0
460	59.5	62.1	53.3	60.1
470	**60.0**	**62.5**	**54.0**	**60.6**
480	60.4	62.9	54.6	61.1
500	61.2	63.6	55.8	61.9
520	61.9	64.2	56.6	62.6
540	62.4	64.7	57.3	63.1
546	**62.5**	**64.8**	**57.4**	**63.2**
560	62.8	65.1	57.8	63.5
580	63.1	65.5	58.2	63.8
589	**63.2**	**65.6**	**58.2**	**63.8**
600	63.4	65.7	58.3	63.9
620	63.6	65.9	58.5	64.1
640	63.7	66.0	58.5	64.1
650	**63.7**	**66.0**	**58.5**	**64.1**
660	63.8	66.1	58.4	64.1
680	63.9	66.3	58.3	64.1
700	64.0	66.4	58.2	64.1

The values required by the Commission on Ore Mineralogy are given in bold.

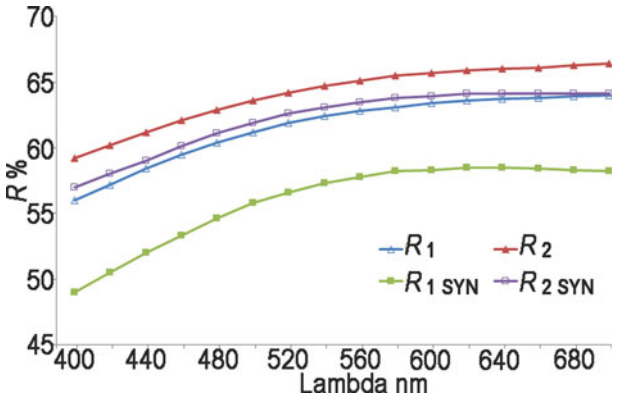

Fig. 3. Reflectance data for natural pampaloite compared to synthetic pampaloite in air. The reflectance values (*R*%) are plotted versus wavelength (λ in nm).

Synthetic analogue

The small size and tiny intergrowths of pampaloite with altaite, frohbergite and native gold prevented its extraction and isolation in an amount sufficient for the relevant crystallographic and structural investigations. Therefore, these investigations were performed on the synthetic AuSbTe.

The synthetic phase AuSbTe was prepared in an evacuated and sealed silica-glass tube in a horizontal furnace in the Laboratory of Experimental Mineralogy of the Czech Geological Survey in Prague. To prevent loss of material to the vapour phase during the experiment, the free space in the tube was reduced by placing a closely fitting silica glass rod against the charge. The temperature was measured with Pt–PtRh thermocouples and is accurate to within ± 3°C. A charge of ~300 mg was carefully weighed out from the native elements. We used, as starting chemicals, gold powder (Aldrich Chemical Co., 99.999% purity), antimony pebbles (Aldrich Chemical Co., 99.999% purity), and a tellurium ingot (Aldrich Chemical Co., 99.95% purity). The starting mixture was first melted at 1000°C for two days, quenched and then ground in an agate mortar under acetone and reheated to

https://doi.org/10.1180/mgm.2018.129 Published online by Cambridge University Press

Table 2. Electron-microprobe analyses of natural and synthetic pampaloite.

Natural sample Sample no.	1 / 1	2 / 1	3 / 1	4 / 1	5 / 1	6 / 1	7 / 1	8 / 1	9 / 1	10 / 1	average
Constituent (wt.%)											
Au	44.14	44.16	44.10	44.05	43.59	43.99	44.42	44.40	44.06	44.44	44.13
Sb	27.44	27.37	27.39	27.38	27.41	27.39	27.61	27.40	27.42	27.57	27.44
Te	28.78	29.20	28.62	28.65	28.37	29.08	29.04	28.42	28.33	28.89	28.74
Total	100.36	100.74	100.11	100.08	99.36	100.46	101.07	100.21	99.81	100.9	100.31
Formula calculated on the basis of 3 atoms per formula unit											
Au	1.00	0.99	1.00	1.00	0.99	0.99	1.00	1.00	1.00	1.00	1.00
Sb	1.00	1.00	1.00	1.00	1.01	1.00	1.00	1.00	1.01	1.00	1.00
Te	1.00	1.01	1.00	1.00	1.00	1.01	1.00	0.99	0.99	1.00	1.00

Synthetic sample Sample no.	17 / 1	18 / 1	19 / 1	20 / 1	21 / 1	22 / 1	23 / 1	24 / 1	25 / 1	29 / 1	32 / 1	average
Constituent (wt.%)												
Au	43.93	43.67	44.68	44.00	43.11	44.12	44.09	44.20	44.78	44.26	43.55	44.03
Sb	27.11	27.38	27.33	27.12	27.15	27.28	27.33	27.22	27.28	27.31	27.36	27.26
Te	29.25	28.93	28.64	28.87	29.38	29.16	29.06	29.35	29.11	29.24	28.92	29.08
Total	100.29	99.98	100.65	99.99	99.64	100.55	100.48	100.77	101.17	100.8	99.83	100.38
Formula calculated on the basis of 3 atoms per formula unit												
Au	0.99	0.99	1.01	1.00	0.98	0.99	0.99	0.99	1.00	0.99	0.99	0.99
Sb	0.99	1.00	1.00	0.99	1.00	0.99	1.00	0.99	0.99	0.99	1.00	1.00
Te	1.02	1.01	1.00	1.01	1.03	1.01	1.01	1.02	1.01	1.01	1.01	1.01

350°C for almost one year. The experimental product was not however homogenous and therefore the sample was heated for an additional nine months at 400°C which resulted in an equilibrated homogenous phase (Fig. 4). The sample was quenched by dropping the capsule in cold water.

X-ray crystallography

Single-crystal diffraction of synthetic pampaloite

A small fragment 33 μm × 22 μm × 14 μm of synthetic AuSbTe was mounted on a glass fibre and examined using a Rigaku Super Nova single-crystal diffractometer with an Atlas S2 CCD detector utilising Mo*K*α radiation, provided by a microfocus X-ray tube and monochromatised by primary mirror optics. The ω rotational scans were used for collection of three-dimensional intensity data. From a total of 2016 reflections, 760 were independent and, 664 were classified as unique with $I > 3\sigma(I)$. Corrections for background, Lorentz effects and polarisation were applied during data reduction with the *CrysAlis* software. Corrections for absorption for spherical sample were applied with the *JANA2006* program (Petříček *et al.*, 2014). The crystal structure was solved with a charge-flipping method using the program *Superflip* (Palatinus and Chapuis, 2007) and subsequently refined by the full-matrix least-squares algorithm of *JANA2006* program (Petříček *et al.*, 2014). The initial crystal structure solution contains three atomic sites in the asymmetric unit. One site was identified as an Au atom, and two sites as Sb atoms. All of the sites are in a general Wyckoff position 8*f* of the space group *C*2/*c*. Considering the composition is AuSbTe, it is obvious that Te should be placed in the structure. Owing to the similarity of X-ray scattering curves of Sb and Te atoms, it is difficult to distinguish these atoms using X-ray diffraction (XRD) data alone. Anisotropic refinement with Te and Sb atoms placed at the positions indicated in Table 3 (i.e. ordered structure), converged to $R = 0.0311$ and $wR = 0.0777$ for 664 reflections. Refinement of the pampaloite structure with inverse occupation of the positions (i.e. Sb on Te site and vice versa) led to the slight increase of R factors to $R = 0.0324$ and $wR = 0.0837$. Refinement of a structure with a random distribution of Sb and Te atoms (i.e. two Sb/Te mix sites with 0.5/0.5 occupancy) yielded $R = 0.0320$ and $wR = 0.0800$. The crystal-chemical environment of Sb and Te positions is very similar (see structure description) and thus cannot be used to decipher the Sb/Te occupancy. Nevertheless, the non-existence of a solid solution of pampaloite in the Au–Sb–Te system (Nakamura and Ikeda, 2002), moderate temperature of synthesis of AuSbTe used in the structure solution, stoichiometry of the crystallographic positions 1:1:1 in the pampaloite structure corresponding to the stoichiometry of the mineral, suggest that there is very likely to be an ordered distribution of Sb and Te atoms in its crystal structure. A certain degree of disorder at Sb and Te positions cannot be ruled out. However, Sb and Te atoms are vital for pampaloite formation; analogous compounds containing only Au and Sb or Te, respectively (i.e. $AuSb_2$ and $AuTe_2$) show different crystal structures (see below). Thus, the structure of pampaloite was refined assuming distinct Sb and Te positions.

By analogy with the montbrayite structure (Bindi *et al.*, 2018), where the Au–Sb substitution was observed, the occupancy of the Au position was also refined (Au versus vacancy). The refinement indicated a fully occupied Au position. All atoms were refined with anisotropic displacement parameters. Refinement for 28 parameters converged to $R = 0.0311$ and $wR = 0.0777$ for 664 reflections. Details of data collection, crystallographic data and refinement for the ordered structure model are summarised in Table 4. Table 5 shows selected bond lengths. The crystallographic information files have been deposited with the Principal Editor of *Mineralogical Magazine* and are available as Supplementary material (see below).

Powder XRD of synthetic pampaloite

The powder XRD pattern of synthetic pampaloite was collected in the Bragg–Brentano geometry on a Bruker D8 Advance diffractometer equipped with the LynxEye XE detector and Cu*K*α

https://doi.org/10.1180/mgm.2018.129 Published online by Cambridge University Press

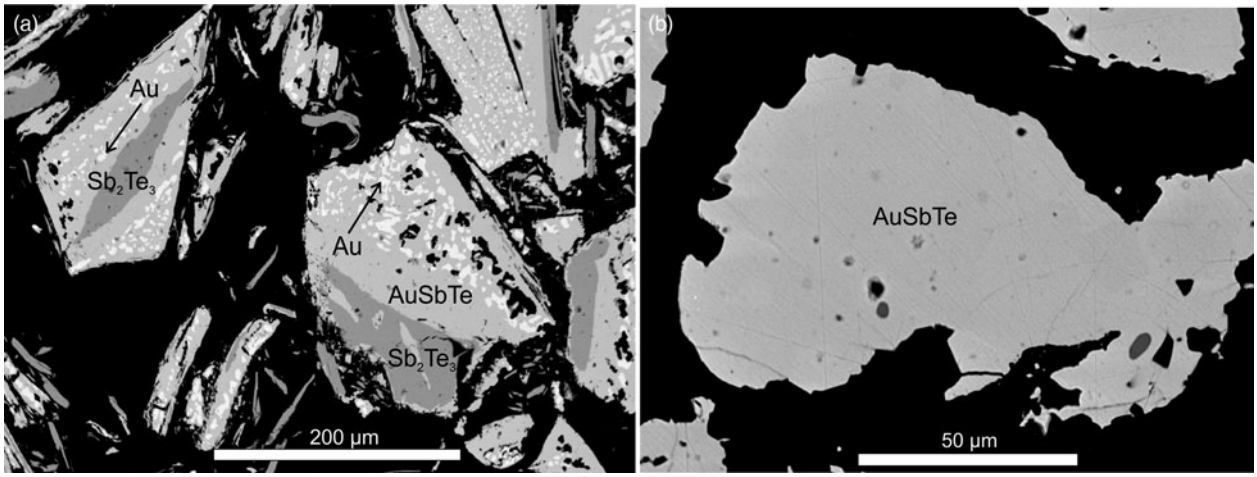

Fig. 4. Synthetic pampaloite (AuSbTe) heated: (*a*) for 12 months at 350°C; and an unequilibrated sample (*b*) heated for an additional 9 months at 400°C until equilibrium was attained.

Table 3. Fractional coordinates and anisotropic displacement parameters (Å^2) for synthetic pampaloite.

Atom	*x/a*	*y/b*	*z/c*	U_{eq}	U^{11}	U^{22}	U^{33}	U^{12}	U^{13}	U^{23}
Au	0.37033(4)	0.2678(1)	0.37232(4)	0.0225(2)	0.0206(3)	0.0234(3)	0.0219(3)	0.0016(2)	0.0034(3)	0.0001(2)
Te	0.30151(8)	0.3407(2)	0.14532(8)	0.0207(3)	0.0175(5)	0.0193(5)	0.0210(5)	0.0006(4)	0.0044(4)	0.0000(4)
Sb	0.47155(8)	0.2838(2)	0.59591(8)	0.0216(3)	0.0205(5)	0.0212(5)	0.0222(5)	0.0010(4)	0.0044(4)	0.0005(4)

Table 4. Crystallographic data for the selected crystal of synthetic pampaloite AuSbTe.

Crystal data	
Ideal formula	AuSbTe
Crystal size (μm)	33 × 22 × 14
Crystal system, space group	Monoclinic *C*2/*c* (15)
Temperature (K)	296
a, *b*, *c* (Å)	11.947(3), 4.481(1), 12.335(3)
β (°)	105.83(2)
V (Å^3)	635.3(3)
Z	8
Calculated density (g cm^{-3})	9.33
μ (mm^{-1})	63.31
Data collection	
Diffractometer	SuperNova
Radiation type, wavelength (Å)	Mo*K*α, 0.7107
Number of frames	
θ range (°)	3.43–29.41
Absorption correction	Empirical
T_{min}, T_{max}	0.023, 0.046
No. of measured, independent and observed [$I > 3(\sigma)$] reflections	2016, 760, 664
R_{int}	0.0249
Index ranges	$-15 < h < 14$, $-6 < k < 5$, $-15 < l < 16$
Structure refinement	
Refinement method	Full matrix least-squares on F^2
Parameters/restrains/constraints	28/0/0
R, w*R* (obs)	0.0311/0.0777
R, w*R* (all)	0.0366/0.0802
GoF (obs)	1.49
$\Delta\rho_{max}$, $\Delta\rho_{min}$ (e^-/Å^3)	2.37/–1.58

Table 5. Selected bond distances (<3.5 Å) in the pampaloite crystal structure.

Au–Sb	2.693(1)	Au–Sb	3.071(1)	Sb–Te	2.829(2)
Au–Sb	2.712(1)				
Au–Te	2.714(1)	Au–Te	3.257(1)	Te–Te	3.553(2)
Au–Te	2.771(1)				

Table 6. Powder diffraction data collection and Rietveld analysis of a synthetic pampaloite.

Data collection	
Radiation type, source	X-ray, Cu*K*α
Generator settings	40 kV, 30 mA
Range in 2θ (°)	15–90
Step size (°)	0.005
Crystal data	
Space group	*C*2/*c* (15)
Unit-cell content	AuSbTe, *Z* = 8
a, *b*, *c* (Å)	11.9634(2), 4.4851(1), 12.3430(2)
β (°)	105.859(3)
V (Å^3)	637.1(5)
Agreement factors (Rietveld refinement)	
R_{Bragg}	0.074
R_p	0.068
R_{wp}	0.089
Weighting scheme	$1/y_o$

radiation. The data were collected in the range from 15° to 90°2θ with a step size of 0.005°2θ and 1 s counting time per step. The structure model obtained from a single-crystal XRD study of synthetic pampaloite was used as a starting structural model in the subsequent Rietveld refinement. The *FullProf* program (Rodríguez-Carvajal, 2006) and the pseudo-Voigt function were used to generate the shape of the diffraction peaks. The refined parameters include those describing peak shape and width, peak asymmetry, unit-cell parameters, and an overall isotropic displacement parameter. In total, 12 parameters were refined. No fractional coordinates were refined. The refinement indicated 1.5 wt.% Sb_2Te_3 impurity in the sample of synthetic pampaloite investigated. Table 6 summarises the results of the Rietveld

https://doi.org/10.1180/mgm.2018.129 Published online by Cambridge University Press

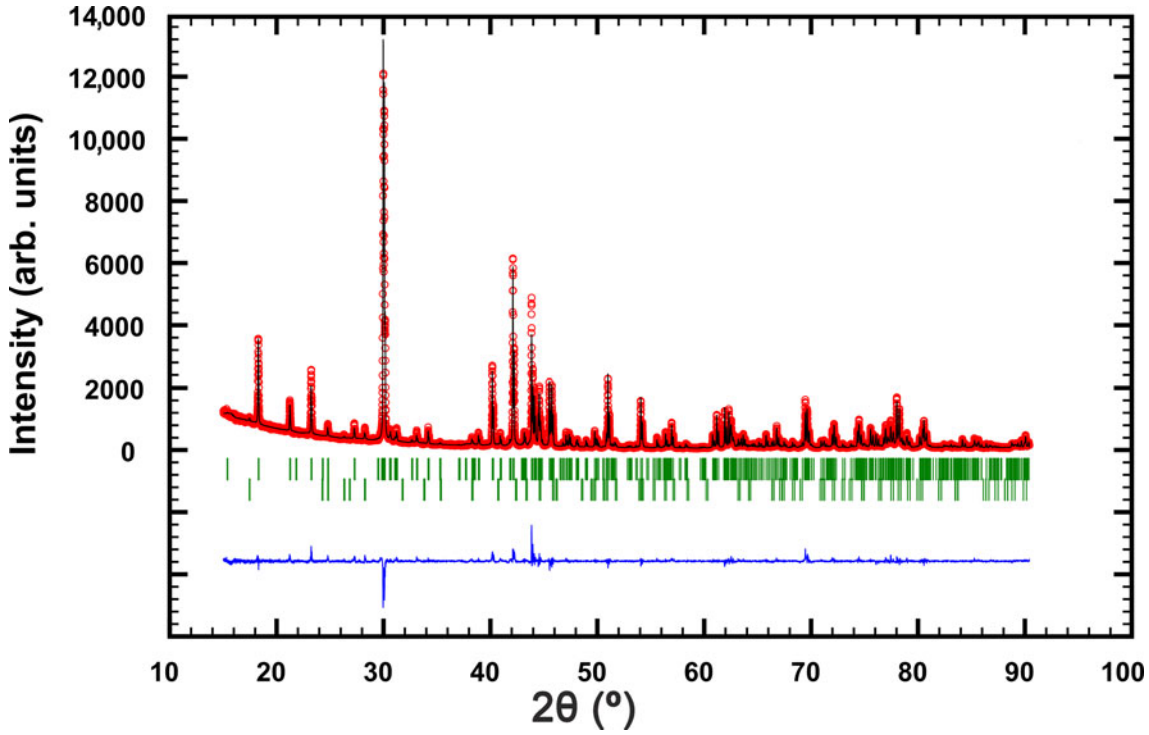

Fig 5. The observed (circles), calculated (solid line) and difference Rietveld profiles for synthetic pampaloite. The upper reflection markers correspond to synthetic pampaloite, and the lower markers to 1.5 wt.% Sb_2Te_3 impurity.

refinement; Fig. 5 shows the final Rietveld plot. Table 7 presents the powder XRD data.

Structure description

The crystal structure of pampaloite is based on deformed hexagonal packing of Sb and Te atoms where a half of the available octahedral voids is filled with Au atoms. As indicated in Fig 6, the Au atom shows 4 + 1+1 coordination by three Sb and three Te atoms with bond distances ranging from 2.693(1) to 3.257(1) Å (Table 5). Consequently, Au atoms form $[AuSb_3Te_3]$ elongated octahedra having Sb and Te atoms in a facial (*fac*) configuration. The coordination environment of Sb and Te atoms is similar. Both atoms have three short contacts with Au showing 2 + 1 bonding scheme. In addition, they form characteristic Sb–Te dumbbells with a bond distance of 2.829(2) Å. Contrary to the Te position, the Sb position shows one additional short contact with Sb at a distance of 3.270(2) Å. The Sb–Te separation of 2.829(2) Å in the pampaloite structure distance is slightly shorter than the Sb–Sb bond distance of 2.908 Å in the structure of native Sb (Barrett *et al.*, 1963) and comparable to that of 2.834 Å observed in native Te (Adenis *et al.*, 1989). Similar bonding distances of 2.84 Å and 2.85 Å were observed between Te and Te atoms in the structure of krennerite Au_3AgTe_8 (Dye and Smyth, 2012) and stützite $Ag_{5-x}Te_3$ (Bindi and Keutsch, 2018), respectively. Comparable bonding distances of 2.879 Å were also observed in the structure of synthetic PdSbTe (Foecker and Jeitschko, 2001), which can be considered as an ordered derivative of the pyrite structure with the [SbTe] dimeric anions. The Sb–Te separations in pampaloite are even shorter than the Sb–Te distances in an octahedral double layer found in Sb_2Te_3 (2.9789(5) and 3.1680(4) Å, Anderson and Krause, 1974).

The $[AuSb_3Te_3]$ octahedra share Sb–Sb, Te–Te and Sb–Te edges and form sheets oriented parallel to $(\bar{1}01)$ planes. The octahedral sheets are connected by Sb–Te dumbbells across the interlayer space (Fig 6). The structure model of pampaloite presented in this work strongly resembles the average structure of calaverite $AuTe_2$ (Bindi *et al.*, 2009; Schutte and de Boer, 1988), sylvanite $AuAgTe_4$ (Pertlik, 1984) and muthmannite $AuAgTe_2$ (Bindi and Cipriani, 2004). In all structures, Au show more or less distorted octahedral coordination.

Whereas the sheets of the edge-sharing $[AuTe_6]$ octahedra in the average structure of calaverite are linked by Te–Te bonds, the sheets of $[AuSb_3Te_3]$ octahedra in the pampaloite structure are connected by a system of Sb–Te bonds. In the sylvanite structure, $[AuTe_6]$ and $[AgTe_6]$ octahedra share form sheets, which are combined to a network by means of Te–Te dumbbells (2.82 Å). Contrary to that, the sheets of $[AuTe_6]$ octahedra in muthmannite are connected by sheets of $[AgTe_6]$ octahedra. Moreover, the structure of calaverite is incommensurately modulated (Bindi *et al.*, 2009; Schutte and de Boer, 1988).

The pampaloite structure crystalises in a unique structure type, no exact structural analogues have been observed. It can be considered as a monoclinic derivative of the CdI_2 structure type. From a chemical point of view, pampaloite is very close to aurostibite $AuSb_2$ and montbrayite $(Au,Ag,Sb,Pb,Bi)_{23}(Te,Sb,Pb,Bi)_{38}$, however its crystal structure differs from the above mentioned minerals. Aurostibite shows a three-dimensional network composed of corner-sharing $[AuSb_6]$ octahedra (Furuseth *et al.*, 1965) whereas pampaloite shows a layered structure. In the montbrayite structure (Bindi *et al.*, 2018), the $[AuTe_6]$ octahedra form edge-sharing octahedral chains along [101], generating empty spaces with Te–Te contacts (from 2.83 to 2.90 Å).

https://doi.org/10.1180/mgm.2018.129 Published online by Cambridge University Press

Table 7. Powder XRD data for synthetic pampaloite (Cu$K\alpha$ radiation).

I_{obs}	I_{calc}	d_{obs}	d_{calc}	*hkl*	I_{obs}	I_{calc}	d_{obs}	d_{calc}	*hkl*	I_{obs}	I_{calc}	d_{obs}	d_{calc}	*hkl*
24	**20**	**4.8460**	**4.8465**	**$\bar{2}02$**	17	17	1.9914	1.9912	$\bar{6}02$	10	9	1.5138	1.5138	$\bar{2}26$
12	7	4.1790	4.1788	110	16	14	1.9818	1.9819	115	9	9	1.4973	1.4973	$\bar{5}17$
18	14	3.8247	3.8248	111	4	3	1.9287	1.9285	$\bar{2}23$	9	10	1.4889	1.4890	$\bar{6}22$
2	2	3.5885	3.5890	$\bar{1}12$	1	1	1.9178	1.9175	$\bar{5}14$	2	2	1.4704	1.4704	$\bar{6}23$
5	4	3.2678	3.2679	112	2	1	1.8929	1.8926	314	3	3	1.4608	1.4606	$\bar{8}04$
100	**100**	**2.9780**	**2.9779**	**$\bar{3}11$**	2	2	1.8894	1.8893	$\bar{4}06$	4	3	1.4183	1.4182	424
50	**47**	**2.9681**	**2.9685**	**004**	2	2	1.8591	1.8591	$\bar{6}04$	6	5	1.3997	1.3996	$\bar{3}31$
4	3	2.7038	2.7040	311	5	4	1.8310	1.8309	404	13	10	1.3521	1.3520	622
4	3	2.6214	2.6216	$\bar{3}13$	2	2	1.8226	1.8227	$\bar{3}16$	10	8	1.3493	1.3493	317
3	2	2.3140	2.3140	114	3	3	1.7941	1.7938	$\bar{4}21$	4	4	1.3108	1.3108	$\bar{6}26$
25	**20**	**2.2424**	**2.2425**	**020**	**18**	**16**	**1.7893**	**1.7893**	**024**	4	3	1.3083	1.3084	$\bar{3}19$
4		2.2036	2.2035	021	1	1	1.7764	1.7764	223	5	4	1.2750	1.2749	333
55	**44**	**2.1441**	**2.1441**	**313**	1	1	1.7687	1.7687	420	3	3	1.2573	1.2572	$\bar{3}35$
3	2	2.0938	2.0936	$\bar{2}21$	14	13	1.6947	1.6946	602	9	8	1.2238	1.2237	119
33	**29**	**2.0629**	**2.0629**	**$\bar{3}15$**	3	2	1.6521	1.6521	$\bar{2}25$	8	9	1.1916	1.1914	911
13	11	2.0517	2.0518	$\bar{2}06$	4	3	1.6305	1.6304	025					
11	10	2.0311	2.0314	$\bar{5}13$	4	3	1.5223	1.5223	423					

The strongest lines are given in bold

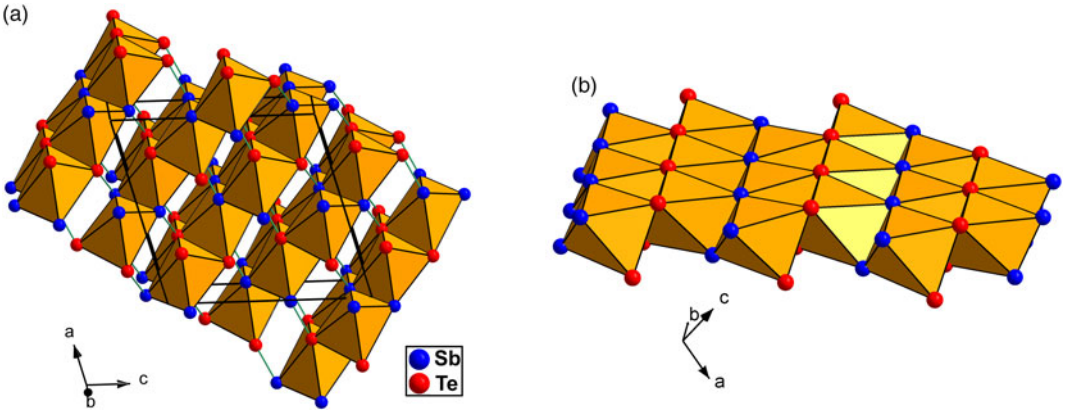

Fig. 6. (*a*) Polyhedral representation of the pampaloite structure emphasising the [$AuTe_3Sb_3$] octahedra. The Sb-Te bonds connecting the layers are indicated by green lines. (*b*) Detailed view of one layer composed of the edge-sharing [$AuTe_3Sb_3$] octahedra.

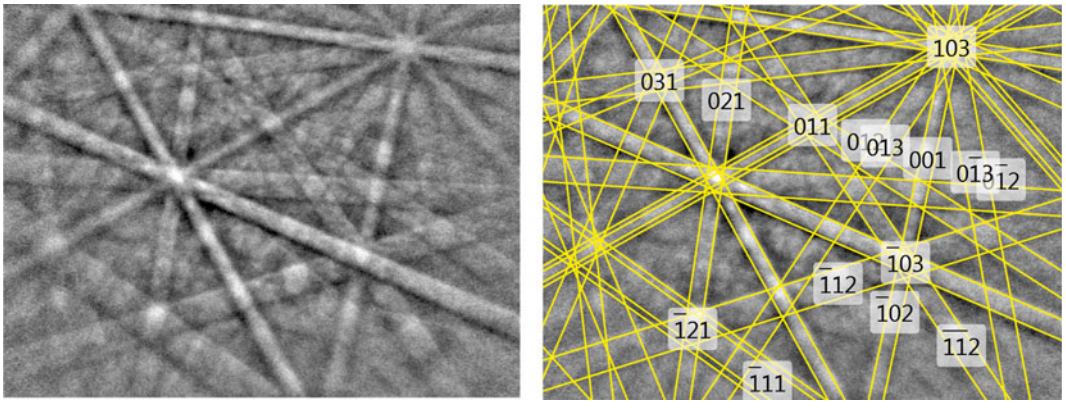

Fig. 7. EBSD image of natural pampaloite; in the right pane, the Kikuchi bands are indexed.

Proof of identity of natural and synthetic pampaloite

The structural identity between the synthetic AuSbTe and the natural material was confirmed by electron back-scattered diffraction (EBSD). For that purpose, we used a TESCAN Mira 3GMU scanning electron microscope combined with an EBSD system (NordlysNano detector, Oxford Instruments). The natural sample was prepared for investigation by re-polishing the surface with colloidal silica (OP-U) for 20 min to reduce the surface damage. The EBSD patterns were collected and processed using a

https://doi.org/10.1180/mgm.2018.129 Published online by Cambridge University Press

proprietary computer program *AZtec HKL* (Oxford Instruments). The solid angles calculated from the patterns were compared with a synthetic AuSbTe match containing 76 reflectors to index the patterns. The Kikuchi patterns obtained from the natural material (seven measurements on different spots on natural pampaloite) were found to match the patterns generated from the structure of synthetic AuSbTe provided by our crystal-structure determination (Fig. 7). The values of the mean angular deviation (MAD) between the calculated and measured Kikuchi bands range between 0.32° and 0.27°. These goodness-of-fit values reveal a very good match; MAD <1° are considered as indicators of an acceptable fit.

The EBSD study, chemical identity and optical properties confirmed the correspondence between natural and synthetic materials and thereby legitimise the use of the synthetic phase for the complete characterisation of pampaloite.

Acknowledgements. The authors acknowledge Ulf Hålenius, Chairman of the CNMNC and its members for helpful comments on the submitted data. This work was supported by the Grant Agency of the Czech Republic (project No. 18-15390S) and through an internal project 331400 from the Czech Geological Survey. The authors are grateful to Dr. Milan Drábek (Czech Geological Survey) for the help with the experimental work and Dr. Zuzana Korbelová (Institute of Geology AS CR, v.v.i.) for carrying out the electron microprobe analyses. JP thanks the project no. LO1603 under the Ministry of Education, Youth and Sports National sustainability program I of the Czech Republic. CJS acknowledges Natural Environment Research Council grant NE/M010848/1 Tellurium and Selenium Cycling and Supply. The reviewer's comments of Luca Bindi, Louis J. Cabri, Peter Leverett and Editor Stuart Mills are greatly appreciated.

Supplementary material. To view supplementary material for this article, please visit https://doi.org/10.1180/mgm.2018.129

References

Adenis C., Langer V. and Lindqvist O. (1989) Reinvestigation of the structure of tellurium. *Acta Crystallographica*, **C45**, 941–942.

Afifi A.M., Kelly W.C. and Essene E.J. (1988) Phase relations among tellurides, sulphides and oxides; II. Applications to telluride-bearing ore deposits. *Economic Geology*, **83**, 377–394.

Anderson T. and Krause H.B. (1974) Refinement of the Sb_2Te_3 and Sb_2Te_2Se structures and their relationship to nonstoichiometric $Sb_2Te_{3-y}Se_y$ compounds. *Acta Crystallographica*, **B30**, 1307–1310.

Barrett C.S., Cucka P. and Haefner K. (1963) The crystal structure of antimony at 4.2, 78 and 298 K. *Acta Crystallographica*, **16**, 451–453.

Bindi L. and Cipriani C. (2004) Ordered distribution of Au and Ag in the crystal structure of muthmannite, $AuAgTe_2$, a rare telluride from Sacarîmb, western Romania. *American Mineralogist*, **89**, 1505–1509.

Bindi L. and Keutsch F.N. (2018) Old defined minerals with complex, still unresolved structures: the case of stützite, $Ag_{5-x}Te_3$. *Zeitschrift für Kristallographie*, **233**, 247–253.

Bindi L., Arakcheeva A. and Chapuis G. (2009) The role of silver on the stabilization of the incommensurately modulated structure in calaverite, $AuTe_2$. *American Mineralogist*, **94**, 728–736.

Bindi L., Paar W.H. and Lepore G.O. (2018) Montbrayite, $(Au,Ag,Sb,Pb,Bi)_{23}(Te,Sb,Pb,Bi)_{38}$, from the Robb–Montbray mine, Montbray, Quebec: crystal structure and revision of the chemical formula. *The Canadian Mineralogist*, **56**, 129–142.

Cabri L.J. (1965) Phase relations in the Au–Ag–Te system and their mineralogical significance. *Economic Geology*, **60**, 1569–1606.

Dye M.D. and Smyth J.R. (2012) The crystal structure and genesis of krennerite Au_3AgTe_8. *The Canadian Mineralogist*, **50**, 119–127.

Endomines AB (2018) Nettisivut https://endomines.com/

Foecker A.J. and Jeitschko W. (2001) The atomic order of the pnictogen and chalcogen atoms in equiatomic ternary compounds T Pn Ch (T = Ni, Pd; Pn = P, As, Sb; Ch = S, Se, Te). *Journal of Solid State Chemistry*, **162**, 69–78.

Furuseth S., Selte K. and Kjekshus A. (1965) Redetermined crystal structures of $PdAs_2$, $PdSb_2$, PtP_2, $PtAs_2$, $PtSb_2$, alpha–$PtBi_2$, and $AuSb_2$. *Acta Chemica Scandinavica*, **19**, 735–741.

Johanson B. and Kojonen K. (1989) Ore mineralogy of gold occurrences in the Hattu schist belt, Ilomantsi, eastern Finland. Current Research 1988, *Geological Survey of Finland, Special Paper*, **10**, 49–52.

Kojonen K., Johanson B., O'Brien H. and Pakkanen L. (1993) Mineralogy of gold occurrences in the late Archean Hattu schist belt, Ilomantsi, eastern Finland. *Geological Survey of Finland, Special paper*, **17**, 233–271

Kojonen K., Johanson B. and Pakkanen L. (1994) Three new telluride minerals from Archean gold deposits in the Hattu schist belt, Ilomantsi, eastern Finland. *Abstract volume in IMA 16th General meeting* in Pisa Italy, 4–9 September 1994, p. 209–210.

Nakamura Y. and Ikeda K. (2002) Isothermal phase relations in the Au–Sb–Te system at 350°C, *Neues Jahrbuch für Mineralogie Monatshefte*, **H6**, 276–288.

Nurmi P.A., Sorjonen-Ward B. and Damstén M. (1993) Geological setting, characteristics and exploration history of mesothermal gold occurrences in the late Archean Hattu schist belt Ilomantsi, eastern Finland. Pp 193–231 in: *Geological Development, Gold Mineralization and Exploration Methods in the Late Archean Hattu Schist Belt, Ilomantsi, Eastern Finland* (P.A. Nurmi and P. Sorjonen-Ward, editors). Geological Survey of Finland, Special Paper **17**.

Palatinus L. and Chapuis G. (2007) SUPERFLIP – a computer program for the solution of crystal structures by charge flipping in arbitrary dimensions. *Journal of Applied Crystallography*, **41**, 786–790.

Pertlik F. (1984) Kristallchemie natürlicher Telluride I. Verfeinerung der Kristallstruktur des Sylvanits, $AuAgTe_4$. *Tschermaks Mineralogischeund Petrographische Mitteilungen*, **33**, 203–212.

Petříček V., Dušek M. and Palatinus L. (2014) Crystallographic Computing System JANA2006: General features. *Zeitschrift für Kristallographie*, **229**, 345–352.

Rodríguez–Carvajal J. (2006) *FullProf.2k Rietveld profile matching & integrated intensities refinement of X-ray and/ or neutron data (powder and/or single-crystal)*. Laboratoire Léon Brillouin, Centre d'Etudes de Saclay, Gif-sur-Yvette, France.

Schutte W.J. and Boer J.L. (1988) Valence fluctuations in the incommensurately modulated structure of calaverite $AuTe_2$. *Acta Crystallographica*, **B44**, 486–494.

Smith D.G.W. and Nickel E.H. (2007) A System of Codification for Unnamed Minerals: Report of the Sub Committee for Unnamed Minerals of the IMA Commission on New Minerals, Nomenclature and Classification. *The Canadian Mineralogist*, **45**, 983–1055.

Vymazalová A., Kojonen K., Laufek F., Johanson B., Stanley C.J., Plášil J. and Halodová P. (2018) Pampaloite, IMA 2017-096. CNMNC Newsletter No. 41, February 2018, page 231; *Mineralogical Magazine*, **82**, 229–233.